# Nucleation of Electrolytically Evolved Hydrogen at an Ideally Smooth Electrode

KESTUTIS V. DAPKUS AND PAUL J. SIDES[1]

*Department of Chemical Engineering, Carnegie-Mellon University, Pittsburgh, Pennsylvania 15213*

Received June 25, 1985; accepted September 6, 1985

Nucleation of electrolytically evolved hydrogen gas bubbles in aqueous sulfuric acid solutions at a mercury pool electrode was investigated. The experiment featured a cell design in which the critical surface for nucleation was continuously renewed and cleaned. Evolution of approximately 0.01 cm (diameter) bubbles from the mercury surface in both 1 *N* and 0.1 *N* solutions was observed at gas supersaturations at least two orders of magnitude below values predicted by nucleation theory and one order of magnitude above saturation. The disparity is attributed to the effects of the intense electric field, over a million V/cm, on the surface tension of the liquid in the electrical double layer where the concentration of hydrogen is the greatest. This effect may be related to general problems associated with water in nucleation experiments. 

## INTRODUCTION

Electrolytic gas evolution comprises production of the molecules at an electrode and their dissolution in the bulk electrolyte, and the ensuing nucleation, growth, and detachment of gas bubbles. While bubble growth and detachment have been studied and previous investigators have mentioned the nucleation activity of surface pits and scratches and other inhomogeneities inevitably present on a solid surface, no one has experimented with nucleation of electrolytically evolved bubbles on an ideal surface. We, by contrast, have studied nucleation of bubbles on an ideally smooth electrode, a mercury pool, which allowed fundamental investigation of nucleation occurring in the presence of the intense electric field in the double layer at an electrode surface.

Bubbles may nucleate when the electrolyte near the electrode is supersaturated with gas as for example, in the electrolytic production of hydrogen. A flux of hydrogen based on a current of a few mA/cm$^2$ is sufficient to supersaturate the liquid since hydrogen is sparingly soluble. When the dissolved gas concentration reaches a critical value, bubbles nucleate and grow. The critical dissolved hydrogen concentration leading to nucleation can be theoretically obtained from classical nucleation theory; however the effectiveness of this theory for electrolytic gas evolution has not been previously examined. We have experimentally tested the prediction of classical nucleation theory for weak gas–liquid solutions when bubbles nucleate in the presence of an electric field associated with a mercury cathode.

Nucleation theory dates from the 1920s when investigators considered the thermodynamics and kinetics of single-component phase transitions (1–8). From this work evolved classical nucleation theory in which density fluctuations engender vapor nuclei that may grow or decay depending on whether the bubble nucleus is larger or smaller than a certain size, termed the critical radius, at which the bubble is in metastable chemical and mechanical equilibrium with its surroundings. The frequency of formation of critical nuclei is inversely proportional to the exponential of the isothermal minimum work required to form such nuclei divided by $kT$. Thus the es-

[1] To whom all correspondence should be addressed.



0021-9797/86 $3.00

sential features of nucleation theory are the expression for the size of the critical bubble nucleus and the formulation of the rate expression as an exponential function of the work associated with the production of a nucleus having this dimension. Blander and Katz have reviewed the derivation of these equations (9).

Electrolytically evolved gas bubbles nucleate from solutions of gas dissolved in a host liquid; hence theory for multiple components is required for this case. Ward (10) obtained an expression for the critical radius for multicomponent systems:

$$R_c = \frac{2\sigma}{\frac{\eta P_\infty}{\nu_1} + \frac{P'C'}{\nu_2 \underline{C}_0} - P'} \qquad [1]$$

where

- $P_\infty$ vapor pressure of solvent at the temperature of the liquid
- $P'$ the external pressure in the liquid
- $\nu_1, \nu_2$ vapor-phase activity coefficients of the solvent and solute
- $C'$ concentration of the gas in the solution surrounding the bubble, expressed as moles of solute per mole of solvent
- $\underline{C}_0$ equilibrium concentration of the gas in the solvent when a flat surface of the solvent is exposed to the gas only at $T$ and $P'$, expressed as moles of solute per mole of solvent
- $\sigma$ surface tension of the liquid–gas interface often assumed equal to the surface tension of the liquid vapor interface
- $\eta$ defined as

$$\eta = \exp\left(\frac{v_1(P' - P_\infty)}{kT} - C'\right)$$

where

- $v_1$ specific volume of the pure solvent.

Tucker and Ward (11) derived a general expression for the critical radius of a bubble for an arbitrary number of volatile solutes present. Their final expression has the same form as [1], but the partial pressure in the denominator is summed over all solutes. The solute gas decreases the critical radius from that of the pure solvent at the same temperature and pressure; therefore the rate of nucleation correspondingly increases. Ward *et al.* (10) have also shown that the rate equation derived for the pure solvent

$$J = Z \exp\left(\frac{-16\pi\sigma^3}{3kT(P'' - P')^2}\right) \qquad [2]$$

where

- $Z$ frequency factor, a very weak function of $T$ and $P$
- $J$ frequency of nucleation $(s \cdot cm^3)^{-1}$
- $P''$ pressure inside the critical bubble

also applies to multicomponent solutions; however, the pressure inside the critical size bubble, $P''$, has two contributions in this case. The dissolved gas exerts a vapor pressure in addition to the vapor pressure of the pure solvent. The increase of $P''$ lowers the critical radius and therefore decreases the maximum attainable supersaturation.

Equation [2] and

$$P'' = \frac{P'C'}{\nu_2 \underline{C}_0} + \frac{P_\infty}{\nu_1}\left[\exp\left(\frac{v_1(P' - P_\infty)}{kT} - C'\right)\right], \qquad [3]$$

a thermodynamic relation between the pressure in the bubble at the critical radius and the dissolved gas concentration (10), are the equations required to predict the rate of nucleation at a given dissolved gas concentration in a given solvent at specified temperature and pressure. Their accuracy is limited by the assumptions of classical nucleation theory. We compare the predictions of these equations for solutions of hydrogen in sulfuric acid with our experimental results.

Heterogeneous nucleation has also been discussed. Apfel (12) derived an expression for the frequency of formation of nuclei at the liquid/liquid interface; the equation resembles its counterpart for the homogeneous case, but

the reversible work contains surface tension values of both liquids and their corresponding interfacial surface tension value. In addition, the prefactor $Z$ in Eq. [2] is less than the prefactor for homogeneous nucleation. Jarvis *et al.* (13) derived an expression for the critical radius of a bubble nucleus for heterogeneous nucleation and a criterion for determining whether homogeneous or heterogeneous nucleation is thermodynamically favorable. The criterion for homogeneous nucleation is

$$(\sigma_1 - \sigma_2)^2 \geqslant \sigma_{12}^2 \qquad [4]$$

where

$\sigma_1$ is the surface tension of liquid 1
$\sigma_2$ is the surface tension of liquid 2
$\sigma_{12}$ is the interfacial tension between the liquids.

If the square of the difference between the bulk phase surface tensions is larger than the square of the interfacial tension, homogeneous nucleation is favored in the phase with the lower bulk surface tension, not at the interface.

Tucker and Ward (11) introduced bubbles slightly smaller and slightly larger than the theoretically predicted size of the critical bubble into a liquid–gas solution. Both bubbles grew although by theory the smaller of the two should have collapsed. They postulated that if an additional solute gas such as nitrogen was present in solution in concentrations on the order of $10^{-2}$ ppm, then this discrepancy could be resolved.

Ward's theory (11) predicted a kinetic limit of superheat lower than that of the pure solvent. For a high gas content, bubbles could nucleate at negative values of the superheat of the solvent. Mori *et al.* (14) used the rising droplet technique to determine the kinetic limit of superheat of a liquid droplet containing dissolved $CO_2$ gas. The three liquids tested were Freon 22, propane, and isobutane. For the isobutane–carbon dioxide system when the gas content was on the order of 30 mole%, they observed kinetic limits of superheat less than the saturation temperature for the pure liquid at the given pressure, that is, bubbles nucleated at pressures exceeding the vapor pressure of the pure solvent at the given temperature as predicted by theory. The propane–carbon dioxide system was the only one where a comparison with theory could be made. They noted that the agreement with theoretical predictions was good at least for $CO_2$ concentrations of up to 30 mole%, which was the highest gas content achieved experimentally.

Forest and Ward (15, 16) isothermally decompressed a suspended ethyl ether droplet containing a known quantity of dissolved nitrogen gas in a host liquid glycerin. The pressure at which a bubble nucleated corresponds to the nucleation pressure $P'$. Accounting for the nonideality of the gas vapor mixture inside the bubble, they found close agreement with theory. Forest and Ward (16) also studied the ethyl ether–nitrogen system under conditions where theory predicts that homogeneous nucleation should occur at negative superheats. Forest and Ward observed homogeneous nucleation at pressures and temperatures above the saturation curve for pure ethyl ether. Since the solubility data for this system was available, they were able to compare their results with theory and in turn found agreement.

Nucleation theory has been successful for many different solvents and the extension of classical nucleation theory for weak gas–liquid solutions has been tested, but the theory has not been tested for gas bubbles nucleating at an electrode because the surfaces of solid electrodes are difficult to control on the scale of distances important to nucleation. Solid surfaces are susceptible to pits and scratches and the surface energy of a solid electrode in contact with electrolyte is not well defined. To study nucleation at an electrified interface, one needs an atomically smooth electrode surface, whose surface energy can be well characterized; hence we chose mercury as our ideally smooth electrode. The surface energy of mercury is well defined and the surface itself is free from unrelieved stresses. Hydrogen gas was electrolytically evolved at a mercury cathode from sulfuric acid solution. At low rates of hydrogen production, the hydrogen mole-

cules were removed from the mercury electrode by convection and diffusion without bubble formation, but when the production of hydrogen exceeded a critical value, bubbles nucleated and grew. This critical dissolved hydrogen gas concentration for nucleation was theoretically obtained from classical nucleation theory and compared to experimentally determined values.

## MATERIALS AND METHODS

Appearing in Fig. 1 is a schematic of the electrolytic cell that consisted of a platinum anode, a mercury pool cathode, electrolyte, and a glass tube that connected the centers of both compartments and directed most of the current to the center of the mercury pool underneath the tube. An interfacial double layer potential greatest at the center of the mercury pool and decreasing radially from the center to the periphery accompanied the nonuniform current distribution on the mercury surface. The interfacial tension therefore increased correspondingly as governed by the Lippmann equation (17); hence the lower surface tension area at the center of the mercury pool flowed outward to relieve the higher surface tension area at the periphery. The steady-state spatially varying potential continuously pumped both the mercury and the electrolytic solution outward at the interface. This radial flow brought fresh mercury and solution continuously to the center of the pool, where the probability for nucleation was the highest, while interfering matter was continuously swept to the cell wall.

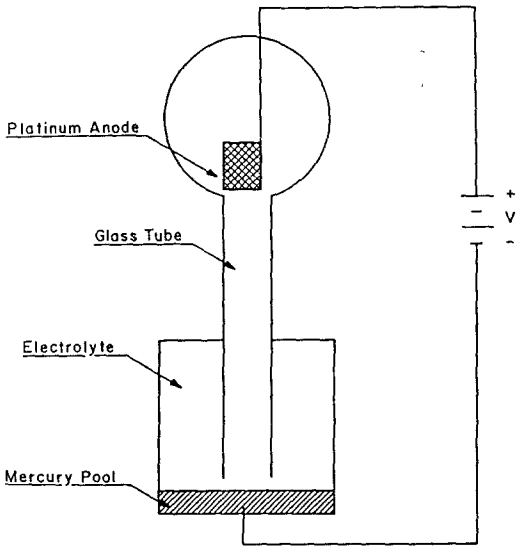


FIG. 1. A schematic of the electrolytic cell for nucleation studies.

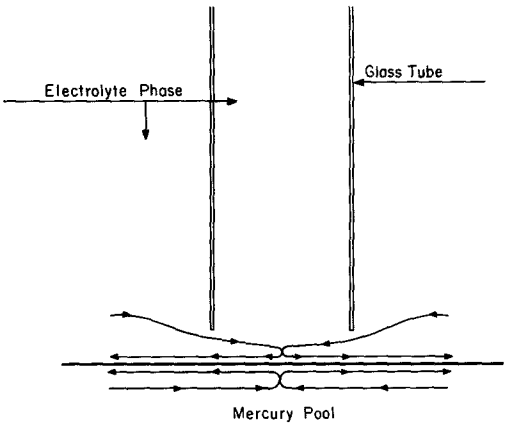


FIG. 2. Qualitative sketch of velocity field, showing the outward radial motion of the interface and the return underneath the edge of the glass tube.

The velocity profiles are sketched qualitatively in Fig. 2. Since the interface flowed radially outward, solution from outside the glass tube flowed back in between the bottom of the tube and the mobile mercury surface to replenish the electrolyte at the center of the mercury pool. This reversal in the velocity was visible when a hydrogen bubble within the center tube was swept out at the interface and returned along the recirculating flow pattern. The surface tension-induced flow continuously renewed the critical area for nucleation at the center where the probability for nucleation was greatest.

Careful preparation of the experiment was necessary to obtain reproducible results in studying the mercury–electrolyte system. In a study of hydrogen overpotential on a mercury cathode, Bowden (18) noted the importance of metal impurities deposited on the cathode

during electrolysis in concentrations less than $10^{-6}$ gram equivalents. He also observed differences in behavior of the mercury–electrolyte system when oxygen was present and when it was excluded from the system (19). Many other investigators have attested to the importance of maintaining an ultraclean, oxygen-free system (20, 21, 18, 22–25). One must use good reagents, remove the oxygen from the solution, and preelectrolyze the electrolyte for removal of impurity ions. Furthermore, platinum used as the anode may poison the mercury (26, 23); the apparatus must separate the platinum anode from the mercury pool cathode. Finally, mercury in contact with electrolyte during the experiment should be polarized cathodically to prevent mercury ions from entering the solution (27).

The mercury, continuous vacuum triple distilled 99.9999% pure instrument grade, was withdrawn from the center of its iron container and stored in glass under hydrogen to avoid oxidation. The electrolytic solution was prepared by combining Ultrex Ultrapure sulfuric acid from Baker (typical metallic impurities in the ppb range) with water obtained from a center deionizing unit and polished with a Millipore four-cylinder water purification train that removed both ionic and organic impurities. The solution was then filtered through a 0.45-$\mu$m membrane filter and pressurized in a PARR pressure vessel with hydrogen to 1800 psig for 20 min in order to free the liquid of any vapor phase centers. Knapp has reported (28) that this pressurization effect lasts for several weeks providing the liquid is not recontaminated.

The hydrogen, obtained from a cylinder at 99.999% minimum purity flowed through a De-Oxo catalytic hydrogen purification unit, thence through molecular sieves to remove water, oil and $CO_2$, and finally through an Oxisorb unit that reduced the oxygen level to less than 0.1 ppm and the water content to less than 0.5 ppm. The hydrogen then flowed through a high purity stainless steel filter, packed with noncontaminating borosilicate fibers capable of removing particles 0.3 microns or larger, and through a 1000-ml glass flask charged with the electrolyte where it was saturated with solution before being fed to the vessels of the apparatus. Contamination of the purified hydrogen with rubber (20, 29) was avoided by using an all glass distribution system. Wilkinson (30) showed that pure hydrogen has no affect on the surface tension of mercury. Likewise, pure hydrogen has no effect on the mercury–water interfacial surface tension. The slight variation of interfacial tension with time, sometimes observed experimentally, is usually attributed to traces of active gases such as oxygen present in the system. In the presence of water vapor, however, the surface tension of mercury decreases with time; hence the hydrogen sent to the mercury reservoir bypassed the saturation vessel.

These precautions governed the construction of the following apparatus, shown in Fig. 3, made entirely out of borosilicate glass with Teflon stopcocks. The important vessels were the bubbler, the preelectrolyzer, the mercury reservoir, and the cell. Auxiliary vessels were the hydrogen and oxygen traps. Prior to assembly, the glassware was washed with detergent, rinsed, and cleaned with hot chromic sulfuric cleaning solution, followed by extensive rinsing with conductivity water to remove dichromate ions. Between each experiment the system was washed with 70°C concentrated sulfuric acid and rinsed with conductivity water. A detailed schematic of the electrolytic cell appears in Fig. 4. The platinum anode, not shown, was separated from the mercury cathode by a coarse glass frit. A 4-cm optical window that allowed observation of the mercury and two smaller 2.5-cm windows used for illumination during filming of the experiments were installed. Also provided were a cooling coil for temperature control and a port for the pressurized Beckman calomel reference electrode that was checked against a standard hydrogen electrode and was found accurate within 1 mV.

In a given experiment, the bubbler was charged with the pretreated electrolyte. Hydrogen bubbled through the solution for a pe-

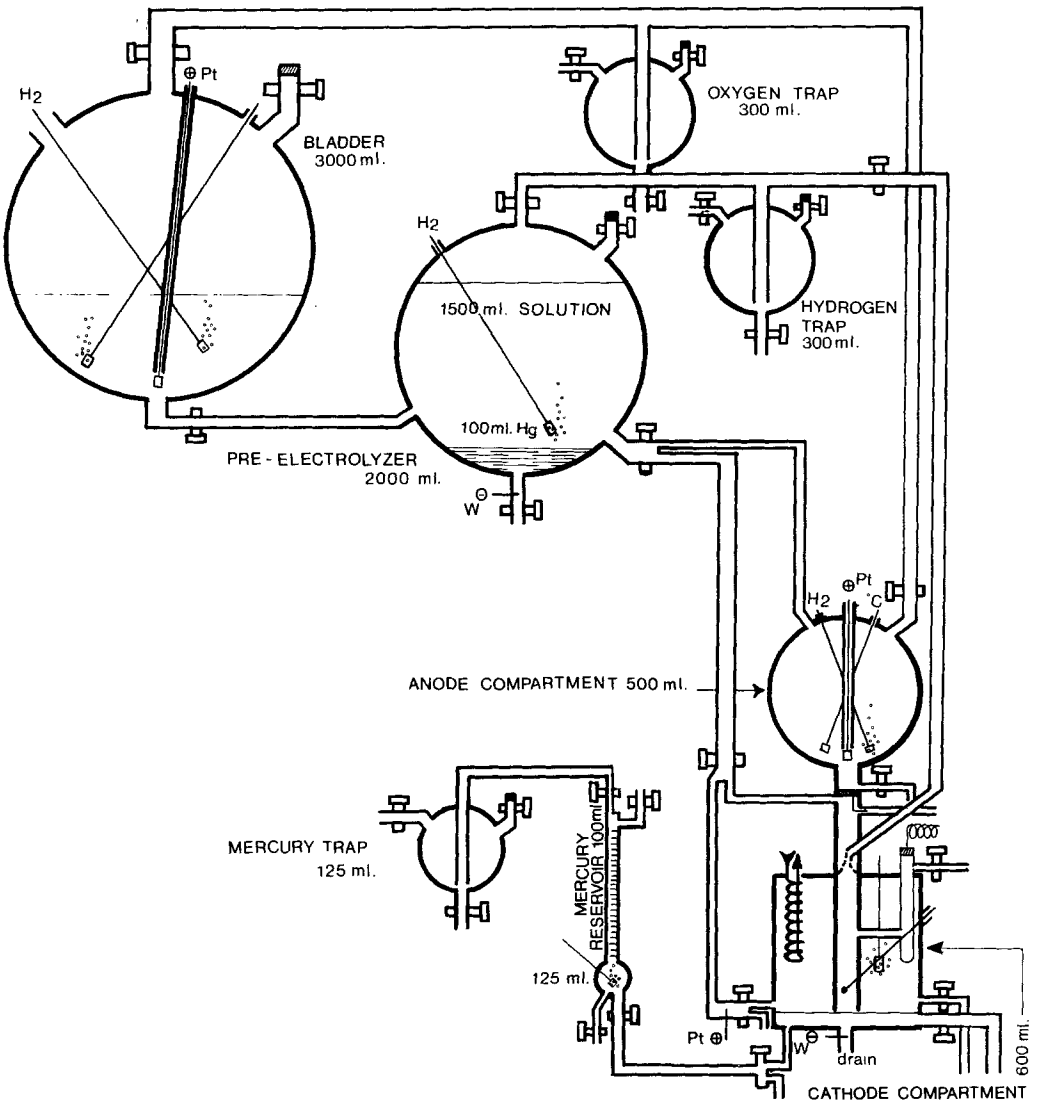


FIG. 3. Experimental apparatus for the nucleation experiment: the bubbler, preelectrolyzer, cell, and auxiliary vessels made with borosilicate glass and teflon stopcocks.

riod of 48 h and flowed through the rest of the system in order to displace any air present during startup. The purged solution then flowed to a vessel containing 100 ml of mercury where it was preelectrolyzed for 72 h before entering the cell where it contacted a known volume of mercury already introduced into the cathode compartment. The mercury was polarized continuously with the aid of a platinum auxiliary electrode to prevent the dissolution of mercury ions during the filling process. Electrolytic current was applied to the cell by a Princeton Applied Research Model 173 potentiostat/galvanostat. The behavior of the mercury surface due to the applied current was recorded on Kodak Tri-X reversal film using a 16-mm Paillard Bolex camera. Because the hydrogen bubbles were about 100 $\mu$m in diameter, we filmed through an American Optical model 55M-2 microscope, at a mag-

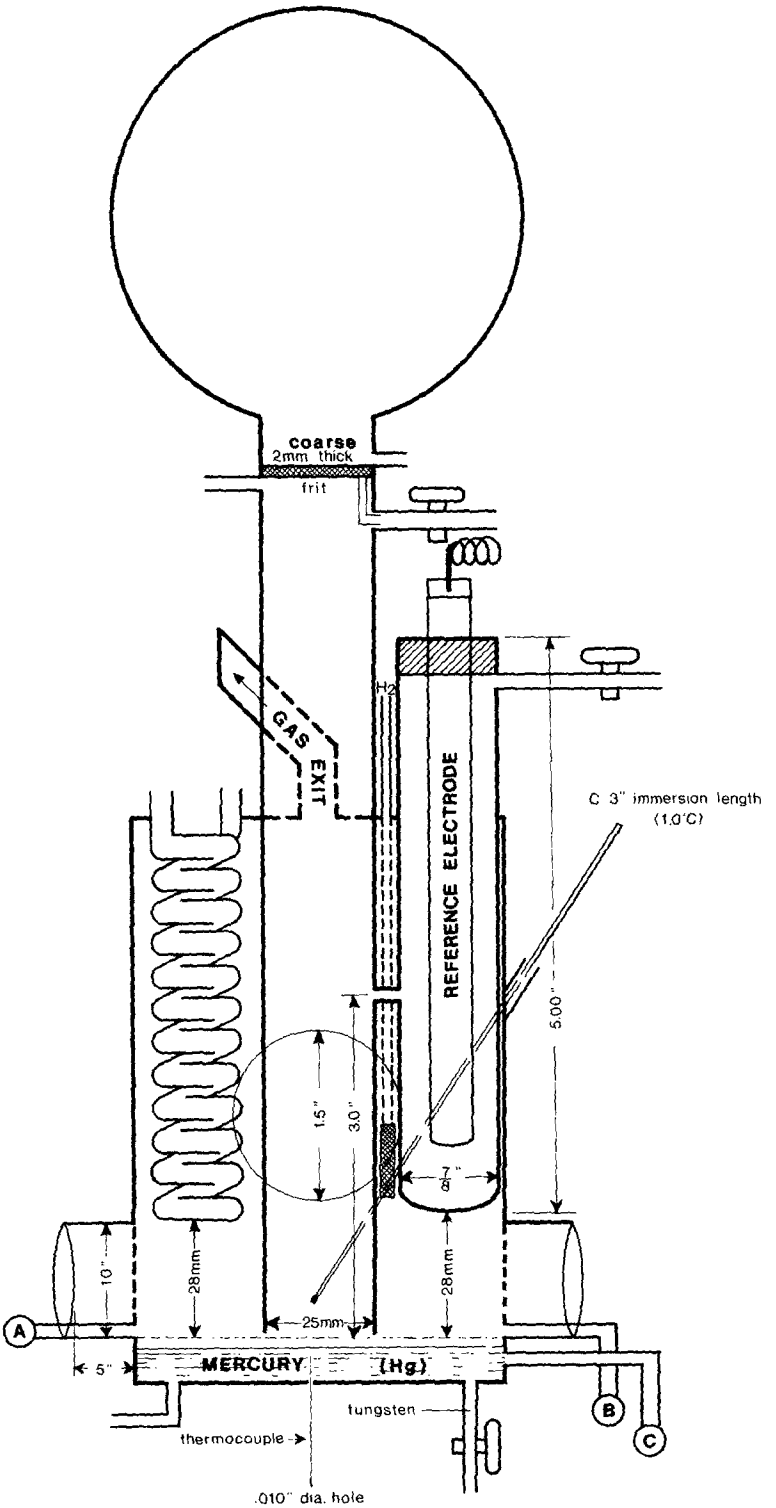


FIG. 4. Electrolytic cell for nucleation study.

nification of 10×. The potential of the mercury pool corresponding to the current passing through the cell was recorded simultaneously on a Nicolet oscilloscope. During the experiments, the mercury pool was always cathodically polarized.

The quality of the electrolyte was checked, as discussed by Conway (31), with cyclic voltammetry on a Pt wire immersed in 2 *N* electrolyte in one of the experiments. The voltammogram exhibited the hydrogen oxidation peaks, the flat intermediate region, and the Pt oxidation peaks observable in clean solution.

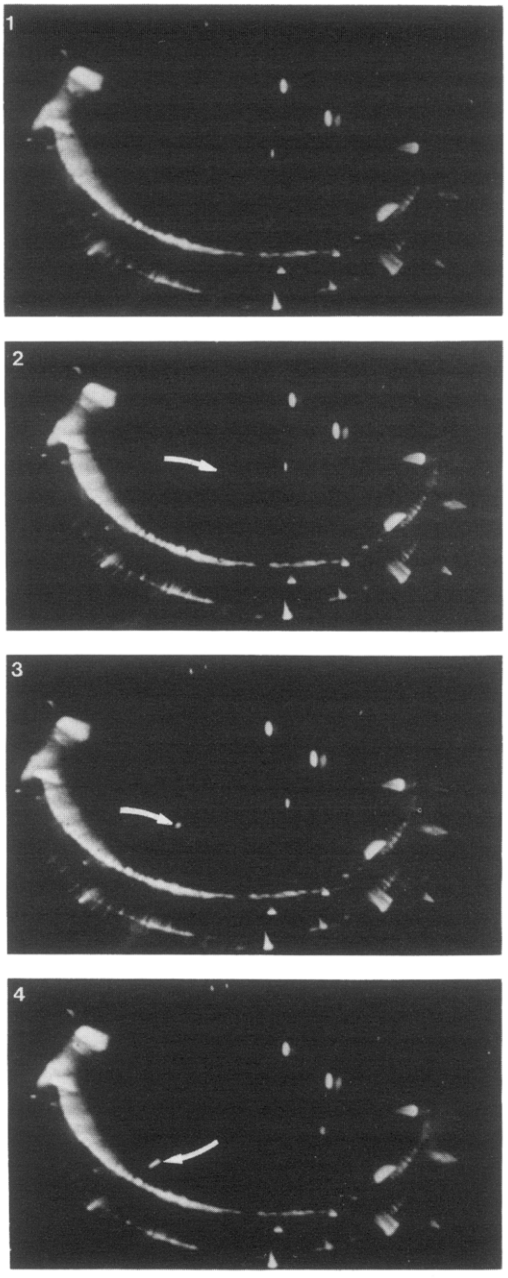


FIG. 5. Appearance and radial motion of a bubble in the nucleation experiment: (1) Only extraneous nonmoving bubbles are present; the bright arc is the bottom edge of the glass tube and the mercury is black (dark field). (2) White arrow points to faint bubble near center. (3) White arrow points to same bubble, several frames later; note the radial translation from the previous frame. (4) The bubble nears the edge. The bubble appears elongated because it travels a certain distance while the camera holds the frame in place.

## RESULTS

### *Experimental Data*

Below certain currents, the mercury surface flowed as described in the introduction, but no bubbles appeared. As the current was increased beyond these levels, small bubbles around 100 $\mu$m in diameter began appearing in the center of the mercury pool and were carried radially outward with the flow. Dark field photographs taken from the films of this phenomenon appear in Fig. 5. The bright arc at the bottom of each frame is the reflection of the curved rim of the glass tube. The frame is 2.54 real cm wide. In the first of the four-photo sequence, only extraneous bubbles attached to the glass tube appear; the black area in the center is the mercury surface. In the second frame a bubble indicated by the arrow appears near the center of the photo and then translates radially as shown in the succeeding frames. (These frames were selected at sequential points from the continuous original; they are not successive frames.) In the final frame the bubble is elongated because its velocity at this point is comparable to the framing rate of the camera.

The frequency of these events was a function of the current. The number of bubbles appearing in a given interval of time were

counted with the aid of the films mentioned in the experimental section. The results appear in Fig. 6 in which the frequency of bubble formation on the ordinate is plotted as a function of current passing through the cell. The value of $J$ is based on the volume of a cylinder having the cross-sectional area of the glass tube and a height of 1 cm; this volume enclosed the events observed. The true volume was smaller than this, because the bubbles nucleated in the center at the surface. Using the larger volume leads to a lower bound on the nucleation rate at a given current density and hence an upper bound on the concentration of dissolved gas at the electrode surface at the onset of nucleation. One might also consider reporting the nucleation rate on the basis of the area underneath the glass tube since the bubbles nucleated at the surface. Shown later is that the use of volume yields a lower bound for the predicted nucleation rate for comparison to an upper bound for the experimentally determined concentration.

Illustrated in Fig. 6 are the effect of electrolyte concentration and experimental reproducibility. The experiment was repeated twice for each of 0.1 $N$ $H_2SO_4$, 0.2 $N$ $H_2SO_4$, 1.0 $N$ $H_2SO_4$, and 2.0 $N$ $H_2SO_4$ as the electrolyte, at 25°C. Concentration affected the nucleation current; bubbles nucleated at lower currents in the more dilute electrolyte. In all four cases the shape of the curve is similar, however, the frequency of bubble formation was more sensitive to current for the more dilute electrolytes. The vertical distance between the experimental points, at a given current, is related to the reproducibility achieved in our experiments. As shown in Fig. 6, the results were reproducible and for most of the solutions were stable for hours.

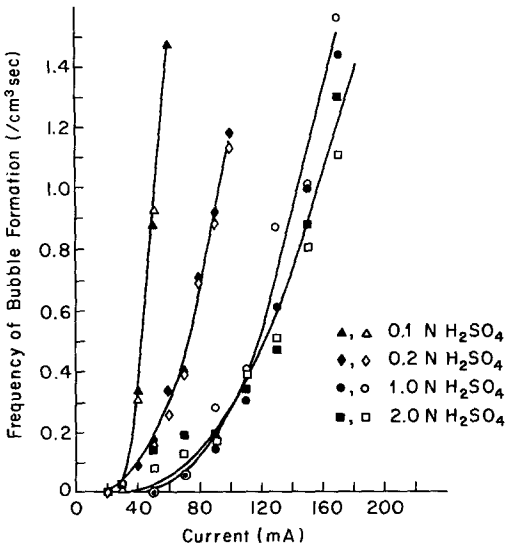


FIG. 6. Frequency of nucleation as a function of current to the cell for four different concentrations of sulfuric acid.

The nucleation current occasionally varied in time for the 0.1 $N$ $H_2SO_4$ electrolyte. In these instances, the nucleation current was steady for 3 h at around 50 mA and then increased with time, which always corresponded to a parallel steady potential followed by a decrease in the potential of the mercury pool. When bubbles were nucleating at the initial lower current densities, the absolute value of the measured potential of the mercury pool was higher than the potential measured for the same current in the higher nucleation current case. For example, in 0.1 $H_2SO_4$ the potential of the mercury pool corresponding to 50 mA was initially −5.41 V. Four hours later the measured potential at this current had fallen to −3.50 V. The drop in required potential accompanied an increase in nucleation current meaning that nucleation required a higher gas concentration. This effect could be reversed by replacing the electrolyte with fresh solution. The nucleation current decreased and the potential likewise increased; the mercury pool was once again in its high potential state. As mentioned earlier, the effect of time on the current and potential was observed only with the 0.1 $N$ $H_2SO_4$ electrolyte and even then only occasionally. The experimental results plotted in Fig. 6, as well as the experimental data used in our analysis were taken from those experiments where no time effect was observed.

The steady-state background concentration of hydrogen required for the analysis was measured by means of a standard hydrogen electrode prepared by platinizing a platinum

electrode in a 10% chloroplatinic acid solution containing 2% lead acetate. The reference electrode was placed inside the electrolytic cell, approximately 5 mm off the mercury surface. The potential measured by this hydrogen electrode was related to the hydrogen concentration by the Nernst equation. For 1.0 $N$ $H_2SO_4$ the saturation concentration equals $7.22 \times 10^{-7}$ gmole $H_2/cm^3$ and for 0.1 $N$ $H_2SO_4$ $C_0$ is equal to $7.73 \times 10^{-7}$ gmole $H_2/cm^3$. A value of 17.8 mV for the potential corresponding to supersaturation of hydrogen in the bulk of the electrolyte was measured at 150 mA steady current. This corresponds to a bulk hydrogen concentration equal to 4 times the saturation concentration.

### *Reduction of Experimental Data*

The essence of the experiment was the determination of the dissolved hydrogen concentration at the surface of the mercury when bubbles were nucleating. Although there was no means for direct experimental measurement of the concentration of hydrogen at the surface of the mercury pool that did not disturb the experiment, measurement of the current and the potential was possible. Therefore, a relationship among the measured current and potential and the desired concentration was required. The complete analysis of the surface concentration of dissolved hydrogen was a complicated three-dimensional convective mass transfer problem; however, an upper bound of the gas concentration was obtained by determining the minimum velocity of the surface and the maximum current density in the crucial region, and then solving the mass transfer problem for convection of the dissolved hydrogen away from the surface.

A lower bound on the radial velocity of the interface was obtained from the films of the experiment, by determining the velocity at which the gas bubbles translated radially to the periphery. The bubbles could not travel faster than the interface; hence their velocity was a minimum velocity of the interface. The position of the bubbles were traced from the films as a function of frame number. Knowing the scale of distance in the frame and the framing rate, we divided the radial translation by the time between each frame. Only bubbles appearing to adhere to the surface and travel with it were used; any bubble that detached and rose from the surface was discarded. Generated in this manner were the velocity data in Fig. 7 for the 1.0 $N$ $H_2SO_4$ and 0.1 $N$ $H_2SO_4$ electrolytes. The experimentally obtained bubble velocities in cm/s are plotted as a function of the radial position along the mercury surface in cm. The center of the mercury pool, where bubbles were nucleating, corresponds to $r = 0$. Likewise $r = 1.255$ cm corresponds to the outside radius of the center glass tube. The lines marked by $a = 5.3$ dyne/cm$^3$ and $a = 4.0$ dyne/cm$^3$ will be discussed later. The scatter in the velocity data was due to measurement error and the fact that bubbles of different sizes traveled at slightly different velocities. The experimental velocities for the 0.1 $N$ $H_2SO_4$ electrolyte were slightly lower than for the 1.0 $N$ $H_2SO_4$ case.

Remaining was determination of the current density distribution and hence the local flux of hydrogen into the solution. Laplace's equation with a Tafel-kinetics boundary condition at the mercury surface was solved (17).

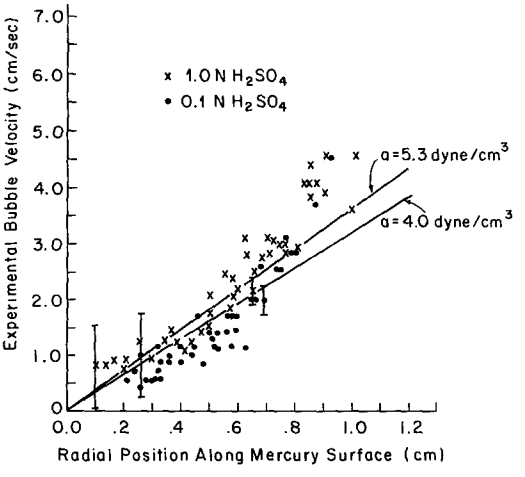


FIG. 7. Experimental bubble velocity . (×) 1 $N$ $H_2SO_4$, (●) 0.1$N$ $H_2SO_4$.

The finite element method was chosen because of the complex geometry of our electrolytic cell and nonlinear boundary conditions. The domain for Laplace's equation, the electrolyte of the cell appearing in Fig. 8, was represented with finite elements. Since only the mercury cathode was important, the model extended to the position of the reference electrode in the center glass tube, that is, only the lower 7.5 cm of the center glass tube was included in the solution domain. The potentials at the top three horizontal nodes therefore represented the potential of the calomel reference electrode. The Galerkin method with a linear polynomial basis function was used for the solution of Laplace's equation. Details of the solution of this problem may be found in Dapkus' dissertation (32).

Required for the calculation was the potential between the mercury and reference electrodes at the onset of nucleation. We chose values corresponding to $J = 1/\text{cm}^3$ s as the nucleation current and potential. Unity for $J$ is often used in the literature and was characteristic of our nucleation experiments. For example, from Fig. 6, the nucleation current for 1.0 $N$ $H_2SO_4$ at 25°C was 150 mA. The potential for this case was 2.733 V relative to the calomel electrode. This procedure permitted a consistent and quantitative method for determining nucleation currents for all the experiments. The current density distributions for 1.0 $N$ and 0.1 $N$ $H_2SO_4$ at 25°C are shown in Fig. 9. The current density is a maximum at the center of the mercury pool, where it reaches a value of 22 $\text{mA/cm}^2$. In both cases the concentration overpotential due to the supersaturation of the solution with hydrogen was only a few millivolts and was neglected in the analysis of the current distribution. The error introduced by this approximation was consistent with the approach of calculating an upper bound on the concentration at the surface and in the end could be shown to be small.

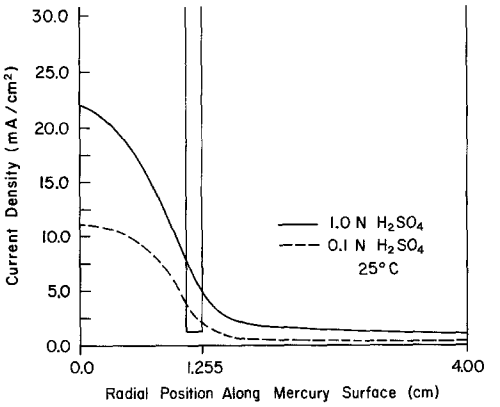


FIG. 9. Current distributions for 1.0 $N$ and 0.1 $N$ $H_2SO_4$.

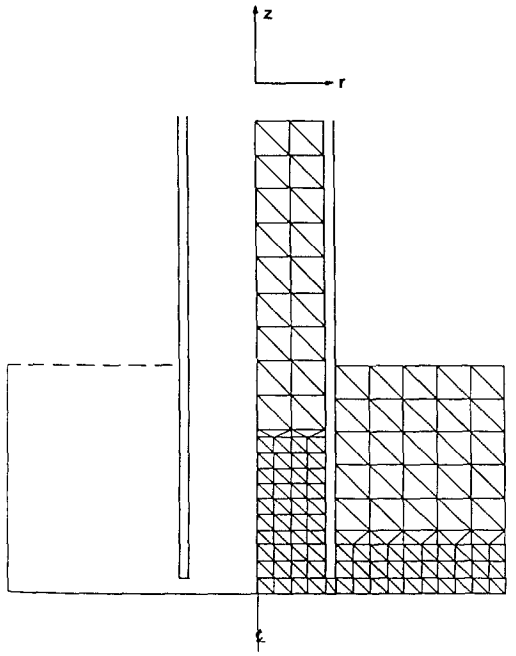


FIG. 8. Finite element model for electrolytic cell.

The nonuniformity of the current distribution, shown in Fig. 9, and the corresponding radial dependence of the double layer potential drove the mercury flow. The interactions among the electrical and surface phenomena for 1.0 $N$ $H_2SO_4$ are shown in Fig. 10. On the left appear the local current density and surface overpotential as a function of radial position along the mercury surface. On the right side appears the interfacial surface tension. The surface tension was obtained from the surface overpotential data and the corresponding

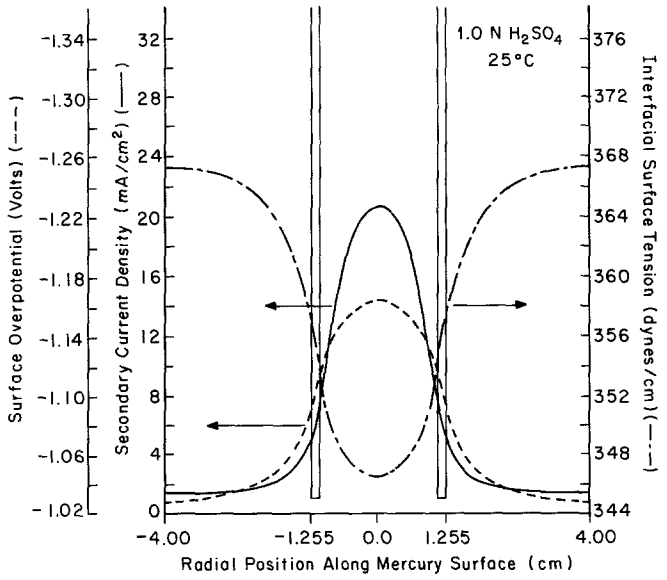


FIG. 10. Effect of nonuniform current distribution on surface overpotential and interfacial tension for 1.0 $N$ $H_2SO_4$.

electrocapillary curves. The interfacial surface tension functionality is a mirror image of the current distribution. At the center of the mercury pool, the interfacial surface tension was a minimum. The highest interfacial surface tension appeared at the periphery of the mercury pool. The lower surface tension area at the center of the mercury pool flowed outward to relieve the higher surface tension at the periphery as discussed earlier. Figure 10 is a summary of the electrical and electrocapillary phenomena within the electrolytic cell. A comparable figure could be generated for the 0.1 $N$ case.

Having the molecular hydrogen flux into solution and surface velocities, we solved the convective diffusion equation to obtain mass transfer coefficients for the transport of hydrogen molecules away from the interface. The analysis was comparable to the rotating disc solution for a surface uniformly accessible to a convective flow with specified flux at the interface (17). Sides (33) has shown that the mercury surface in this geometry is uniformly accessible if the interfacial surface tension varies as the square of the radius, the coefficient of the radial term being given by $a/2$. In this special case the Navier–Stokes equations decouple, permitting analysis. The validity of approximating the flow as uniform accessibility of the surface in the center of the pool has been verified by comparing the theoretically predicted velocities with the experimentally determined velocities (32). The lines marked by $a$ in Fig. 7 are velocities predicted for the indicated values of $a$, as outlined by Sides (33), that were derived from the surface tension profiles shown in Fig. 10. One can show that the mass transfer coefficients calculated from the solution of the convective mass transfer equation are (32)

$$k_1 = 2D_1\left(\frac{m_1 Sc_1}{\pi}\right)^{1/2}\left(\frac{\rho_1 a_1}{\mu_1^2}\right)^{1/3} \qquad [5]$$

and

$$k_2 = 2D_2\left(\frac{m_2 Sc_2}{\pi}\right)^{1/2}\left(\frac{\rho_2 a_2}{\mu_2^2}\right)^{1/3}. \qquad [6]$$

The fluxes of dissolved hydrogen into each of the two phases are

$$\frac{i_1}{nF} = k_1(C_{s1} - C_{\infty 1}) = N_1 \qquad [7]$$

and

$$\frac{i_2}{nF} = k_2(C_{s2} - C_{\infty 2}) = N_2 \qquad [8]$$

where

$N_1$ represents the mass transfer in the aqueous phase;

$N_2$ represents the mass transfer in the mercury phase.

Allowing for mass transfer in both phases, the total current can be written as

$$\frac{i}{nF} = N_1 + N_2$$

$$= (k_1 + k_2)C_s - k_1C_{\infty 1} - k_2C_{\infty 2} \qquad [9]$$

where $[C_s = C_{s1} = C_{s2}]$. Solving for $C_s$, we obtain

$$C_s = \frac{(i/nF) + k_1C_{\infty 1} + k_2C_{\infty 2}}{k_1 + k_2}. \qquad [10]$$

Using the values in Table I, we obtained the values for $k_1$ and $k_2$, listed also in Table I, from Eq. [2] and [3]. The value of $C_{\infty 1}$, the bulk concentration of dissolved hydrogen in the aqueous phase, differed from the equilibrium saturation concentration of hydrogen as discussed in the experimental section. The value was $2.9 \times 10^{-6}$ gmole/cm$^3$ which corresponded to an equivalent pressure of 4 atm. Data on the background concentration of hydrogen in mercury, $C_{\infty 2}$ were not obtained; we calculated the maximum value of the surface concentration by assuming a concentration equal to $C$.

Substituting a current density of 22.4 mA/cm$^2$ into Eq. [10], we found that the experimentally obtained surface concentration of hydrogen at the onset of nucleation for 1.0 $N$ $H_2SO_4$ was at most $1.1 \times 10^{-5}$ for a supersaturation ratio at nucleation of 16 atm. Likewise the experimentally obtained surface concentration of hydrogen for 0.1 $N$ $H_2SO_4$ was at most $7.2 \times 10^{-6}$ for a supersaturation ratio at nucleation of 9.3.

### *Experimental Results and Predictions from Classical Nucleation Theory*

We calculated the value of $C'$ predicted by nucleation theory by solving Eqs. [2] and [3]

TABLE I

Physical Properties for 1.0 and 0.10 $N$ Sulfuric Acid and Mercury

| | | 0.1 $N$ $H_2SO_4$ | 1 $N$ $H_2SO_4$ | Mercury |
|---|---|---|---|---|
| $D_i$ | cm$^2$/s | $4.7 \times 10^{-5}$ | $4.2 \times 10^{-5}$ | $1 \times 10^{-5}$ |
| $m$ | — | 0.271 | 0.271 | 0.66 |
| Sc | — | 201 | 252 | 113 |
| $\rho$ | g/cm$^3$ | 1.00 | 1.03 | 13.5 |
| $a$ | dyn/cm$^3$ | 4.0 | 5.3 | 4.0, 5.3 |
| $\mu$ | g/cm s | $9.54 \times 10^{-3}$ | $1.09 \times 10^{-2}$ | $1.53 \times 10^{-2}$ |
| $n$ | — | 2 | 2 | |
| $F$ | C/eq | 96,487 | 96,487 | |
| $k_1$ | cm/s | $1.39 \times 10^{-2}$ | $1.40 \times 10^{-2}$ | |
| $k_2$ | cm/s | $6.0 \times 10^{-2}$ | $6.6 \times 10^{-2}$ | |
| $C_{\infty 1}$ | gmole $H_2$/cm$^3$ | $3.1 \times 10^{-6}$ | $2.89 \times 10^{-6}$ | |
| $C_0$ | gmole $H_2$/cm$^3$ | $7.73 \times 10^{-7}$ | $7.22 \times 10^{-7}$ | |
| $\underline{C}_0$ | gmole $H_2$/gmole | $1.32 \times 10^{-5}$ | $1.40 \times 10^{-5}$ | |
| $\sigma$ | dyn/cm | 72.3 | 72.0 | |
| $Z$ | 1/cm$^3$ s | $2.5 \times 10^{29}$ | $2.5 \times 10^{29}$ | |
| $\nu_1$ | — | 1.0 | 1.0 | |
| $\nu_2$ | — | 1.0 | 1.0 | |
| $P_\infty$ | dyn/cm$^2$ | $3.1 \times 10^4$ | $3.2 \times 10^4$ | |
| $v_1$ | cm$^3$/molecule | $3.0 \times 10^{-23}$ | $3.0 \times 10^{-23}$ | |

simultaneously for $C'$ and $P''$. Table I contains values for the relevant physical properties for the two concentrations of $H_2SO_4$. The critical concentrations of hydrogen were calculated by using the volumetric prefactor $Z$ in 2, 2.5 $\times 10^{29}/cm^3$ s, that was the value of $Z$ used by Volmer (10) for ethyl ether. A value for $Z$ obtained from an equation given by Blander and Katz (9), 2.12 $\times 10^{31}/cm^3$ s (32), yielded a value for the predicted critical hydrogen concentration that differed by only 3%. Use of a prefactor reflecting an area-based nucleation rate, having a value seven orders of magnitude lower, led to a higher value of the predicted concentration; therefore the volume-based prefactor was used to obtain a lower bound for the predicted concentration.

Summarized in Table II are the results of the calculations and experiments. Reported are the lower bounds of supersaturation of hydrogen as predicted by classical nucleation theory, using a three dimensional prefactor, and the upper bounds of the concentrations as found in the experiment.

## DISCUSSION

The appearance of bubbles at the center of the cell on the surface of the mercury pool marked nucleation. At the low currents, where no bubbles were nucleating, the production rate of hydrogen molecules at the mercury surface was low enough so that gas did not supersaturate the solution beyond a critical amount. With increasing current, however, diffusion and convection were unable to keep the dissolved hydrogen concentration below a critical value at which bubbles nucleate at an observable frequency. Bubbles nucleated and grew rapidly to visible size. The essential results of our experimental analysis for the upper bound to the surface concentration of hydrogen at the onset of nucleation are summarized in Table II for 1.0 $N$ $H_2SO_4$ and 0.1 $N$ $H_2SO_4$. The upper bounds of the experimental results for both electrolyte concentrations were lower than the theoretical predictions by two orders of magnitude; the hydrogen bubbles were nucleating at much lower supersaturations than predicted by theory. Reasons for this discrepancy could be experimental artifacts, incorrect theory, or an effect of the electric field in the double layer.

TABLE II

Summary of Results for 1.0 and 0.10 $N$ Sulfuric Acid

| | 0.1 $N$ $H_2SO_4$ | 1 $N$ $H_2SO_4$ |
|---|---|---|
| $C_0$ gmole/$H_2$/cm$^3$ | $7.7 \times 10^{-7}$ | $7.2 \times 10^{-7}$ |
| $C'_{exp}$ gmole $H_2$/cm$^3$ | $7.2 \times 10^{-6}$ | $1.1 \times 10^{-5}$ |
| $C'_{exp}/C_0$ | 9.3 | 16 |
| $C'_{th}$ gmole $H_2$/cm$^3$ | $1.1 \times 10^{-3}$ | $1.1 \times 10^{-3}$ |
| $C'_{th}/C_0$ | $1.5 \times 10^3$ | $1.5 \times 10^3$ |

The results are trustworthy because precautions were used in the experiment including use of clean reagents, careful deoxygenation of the electrolyte, filtration, pressurization, and because the design of the cell produced a radial motion of the interface which continuously renewed the critical area for the experiment. If the rate of nucleation had depended on the rate at which motes were brought to the surface from the bulk, a weak function of the current, the curves in Fig. 6 would have had smaller slopes; there would have been a more gradual increase of nucleation current with cell current. If the results had depended on the adsorption of an organic at the interface, the curves would either have been not reproducible or would have been indistinguishable. The reproducibility and consistency of change from the 0.1 $N$ solution to 2 $N$ are a pattern unlikely to be preserved if uncontrolled substances were vitiating the results.

Heterogeneous nucleation was considered. Using the criterion derived by Jarvis *et al.* (13), Eq. [4], one can show that homogeneous nucleation was thermodynamically favored for this system because the surface tension of the mercury and the interfacial tension are large compared to the surface tension of water. Although homogeneous nucleation was favored, the hydrogen gas bubbles nucleated within the electrical double layer associated with the mercury electrode because the surface of the

mercury was the source for hydrogen molecules and hence their concentration was greatest there. Thus the hydrogen bubbles probably nucleated in the presence of a strong electric field in the double layer.

Several assumptions were made in solving Eqs. [2] and [3] for $C'$. The value of the surface tension was the liquid–vapor surface tension. Hirth (34) pointed out that quasiequilibrium adsorption of hydrogen at the bubble interface may reduce bulk surface tension by 20%. Using this reduced figure in the calculation of the critical concentration reduces the predicted concentration to 1000 atm, still two orders larger than the observed value. Also assumed was that the macroscopic value of the surface tension applies for the critical size nucleus even though this nucleus has a radius of only 1.0 nm and may contain only 20–30 molecules, which is an inherent problem in classical nucleation theory. The activity coefficients of the solute and solvent in the gas–vapor mixture were assigned values of unity. Analysis of the phase equilibria in this system showed that the term corresponding to the water vapor could be neglected and the activity coefficient of the hydrogen was 2.4, which would have the effect of increasing the supersaturation ratio; hence use of unity was consistent with the lower bound approach.

Aqueous solutions have been troublesome in nucleation experiments in the past. As mentioned in the introduction (9), superheats of nearly 198°C for boiling nucleation experiments have been predicted but the highest obtained were 175°C. Our results indicated an extreme of this discrepancy. The unpredictable behavior of water and the discrepancy in our results may be related, as discussed below.

Perhaps classical nucleation theory and our experimental results disagreed, as evident in Table II, because the bubbles nucleated within the electrical double layer associated with the mercury pool where the strong electric field may have affected the liquid's properties on the microscale. For example, the electric field may have affected the surface tension that appears as an argument, raised to a power of three, in the exponential rate function in the nucleation equation. A lower surface tension within the double layer would be consistent with our experimental results.

The double layer consists of the adsorbed layer of water molecules and the charge-separation region extending into solution. Because of the excess negative charge of the mercury pool, there is an excess of water dipoles with their positive, hydrogen ends pointing toward the mercury. If the Inner Helmholtz Plane (IHP) is defined as the line drawn through the center of the first row of adsorbed water molecules and the diameter of a water molecule is roughly 0.31 nm, the IHP is 0.155 nm away from the mercury surface. The Outer Helmholtz Plane (OHP) is drawn through the center of the closest approach of the solvated hydrogen ions. The diffuse part of the double layer extends from the OHP into the solution. As the concentration of hydrogen ions in the bulk increases, this diffuse part of the double layer becomes more compact. The electric field within the double layer, which can be on the order of MV/cm, can be calculated by solving the Poisson–Boltzmann equation for the electric potential with boundary conditions of specified potential at the OHP and infinity. For mercury, the potential at the OHP can be calculated from the slope of electrocapillary curves through the Lippmann equation and the value at infinity assigned to zero.

The potential at any point within the diffuse layer for a 1:1 electrolyte is given by (35)

$$\phi(x) = \left(\frac{4RT}{|z|F}\right)\tanh^{-1}\left(\exp\left(P - \frac{x}{\lambda}\right)\right) \quad [11]$$

with

$$P = \ln\left(\tanh\left(\frac{|z|F\phi_{ohp}}{4RT}\right)\right) + \frac{x_{ohp}}{\lambda}$$

where

- $\phi$ potential at any point within the diffuse region of the double layer
- $x$ distance from the mercury surface in the aqueous phase
- $z$ charge number

$F$ Faraday's constant

$\lambda$ Debye length, 0.35 nm for 1 $N$ acid, 0.10 nm for 0.1 $N$

$\phi_{ohp}$ potential at the outer Helmholtz plane

$x_{ohp}$ distance of the outer Helmholtz plane from the mercury surface.

Knowing the position and potential of the OHP allowed Eq. [11] to be solved for the variation in potential. Grahame (36) derived a corresponding equation for a 1:2 electrolyte. Sulfuric acid is an intermediate case between a 1:1 electrolyte and a 1:2 electrolyte, because of the partial dissociation of the bisulfate ions. The actual ionic concentrations for 1.0 $N$ $H_2SO_4$ are 0.635, 0.366, and 0.135 g-mole/liter for the hydrogen, bisulfate, and sulfate ions, respectively. Likewise, for 0.1 $N$ $H_2SO_4$ the ion concentrations were calculated to be 0.0683, 0.0317, and 0.0183 gmole/liter. As the concentration of $H_2SO_4$ decreases the electrolyte approaches the behavior of a 1:2 electrolyte. At the concentrations of our experiment, sulfuric acid more closely resembles a 1:1 electrolyte than a 1:2, so the equations for the former are used to provide an approximation of the electric field variation in the double layer.

The resulting potential and electric field variations for 1.0 $N$ $H_2SO_4$ and 0.1 $N$ $H_2SO_4$ have been calculated using Eq. [11] and the results appear in Fig. 11. Included in Fig. 11 are the size and hypothetical position of the critical size bubble, 0.96 nm in radius. The bubble contacts the adsorbed water molecules, but does not displace them. The potential for 1.0 $N$ $H_2SO_4$ within the compact double layer varies linearly with distance, from $\phi$ ($x$ = 0) = −1.163 V to $\phi$ ($x$ = 0.3 nm) = −0.067 V. This corresponds to a uniform electric field of magnitude $-2.3 \times 10^6$ V/cm. This linear potential drop is the true surface overpotential representing the potential available for driving the electrochemical reaction. At increasing distances from the mercury surface, the exponential term in Eq. [11] decreases. Because of the high ionic strength of 1.0 $N$ $H_2SO_4$, the variations in potential and electric field decrease to a tenth of their highest values at 1.2 nm; hence the critical size bubble is somewhat larger than the diffuse double layer thickness for 1.0 $N$ $H_2SO_4$. The critical radius for the 0.1 $N$ $H_2SO_4$ electrolyte is roughly the same as calculated for 1.0 $N$ $H_2SO_4$, namely 0.96 nm, because the surface tension, the important solution parameter, does not change significantly for the more dilute concentration. Although the radius of the critical size bubble does not change, the environment of the critical size bubble is different in these two cases. The critical size bubble for the 0.1 $N$ $H_2SO_4$ electrolyte is smaller than the distance over which the potential and electric field vary.

Figure 11 shows that the environment under which the critical-size bubble grows is different for different electrolyte concentrations. If the electric field does have an appreciable effect on the physical properties of the electrolyte within the double layer, the experimentally obtained critical supersaturation concentra-

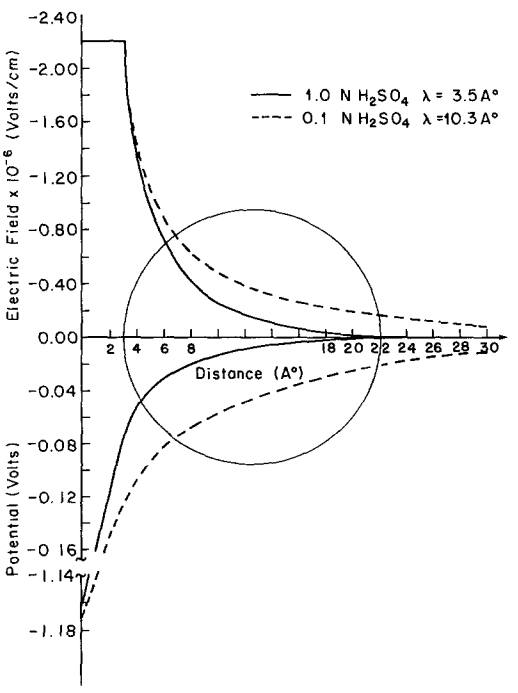


FIG. 11. Critical size bubble within the electrical double layer.

tion, $C'_{exp}$, might depend on the electrolyte concentration. According to Fig. 6, there is a consistent effect of concentration, though the differences among the various concentrations is small compared to the discrepancy with nucleation theory.

Perhaps some insight into the effect of an electric field on surface tension may be gained by considering the following surface tension formula derived by Kirkwood and Buff (37).

$$\sigma = \frac{\pi n_1^2}{8} \int_0^\infty r^4 V'(r) g_l(r) dr \qquad [12]$$

where

- $r$ is the radial distance
- $V'(r)$ is the derivative of the potential of interaction
- $g_l(r)$ is the equilibrium radial distribution function of the liquid phase.

Although Eq. [12] cannot be easily applied to electrolytes because the coulombic interactions cause the integral to diverge, it nevertheless expresses the relationship between surface tension and the energy of interaction between molecules. If the strong electric field affects the average orientation of the water dipoles the potential of interaction would change correspondingly. In addition the radial distribution function, being a sensitive function of this potential, would also be affected. According to Eq. [12] the presence of the electric field would result in a change in the surface tension value as experimentally observed by Schmid *et al.* (38). They measured the surface tension values of NaCl solutions in the presence of an applied electric field and observed a decrease in the measured surface tension as the magnitude of the electric field increased. This decrease was observed for both positive and negative electric fields, however, it was more pronounced for the latter case. The highest electric field achieved by Schmid *et al.* was 6700 V/cm, which corresponded to a reduction in the value of the surface tension of approximately 0.15 dyne/cm. This should be compared with our value for the electric field at the outer Helmholtz plane of −2.3 million V/cm. Schmid's plot of the relative change in the surface tension as a function of the magnitude of the electric field suggests a quadratic dependence of the reduction in surface tension on the electric field.

Jalaluddin and Sinha (39) found that the maximum attainable superheat for methanol, isopropanol, and methyl ketone decreased by as much as 20°C and more with the application of an electric field; however, no effect was observed for benzene. Other investigators have examined the effect of an electric field both experimentally and theoretically (40–47). Rusanov and Kuzmin (48) included this effect into nucleation theory.

Perhaps the poor results usually obtained for water in nucleation experiments (49, 12) are related to the electrical effect of the electrical double layer on nucleation. If the aqueous phase contains any particulates, then a double layer is present at the particle's surface. The electric field would reduce the surface tension of water within this double layer, which would result in a weak spot in the water where a bubble could nucleate. Prepressurization of the liquid would not prevent this effect. Nonpolar organic liquids would not exhibit this effect since their ionic concentrations are very low and there would be no tendency for the molecules to orient themselves with the field.

## SUMMARY

A novel experiment for studying nucleation of electrolytically evolved hydrogen bubbles at an ideal electrode surface has been presented. Upper bounds to the critical supersaturation concentration for the 1.0 $N$ $H_2SO_4$ and 0.1 $N$ $H_2SO_4$ electrolytes were calculated from experimental data. Nucleation was observed at much lower concentrations than predicted.

The possibility of nucleation occurring heterogeneously on the mercury surface has been ruled out for the following reasons. The mercury was withdrawn from the interior of the reservoir as a precaution against impurities and the electrolyte was extensively pretreated.

In addition the surface tension induced flow pushed any interfering matter away from the center of the mercury pool, to the periphery. Particles would have remained there since they would not have been wetted by the mercury. The gas bubbles must have been nucleating homogeneously in the electrolyte at the electrode surface where the concentration of dissolved gas was the highest. In addition, if bubbles were nucleating on impurities present on the mercury surface we would have expected the frequency of nuclei formation to be substantially constant as a function of current density because the rate of nucleation would then be controlled more by the rate at which the impurity is brought to the surface. As shown in Fig. 6, however, we observed a strong dependence of the frequency of nucleation with current; furthermore, this dependence was reproducible.

From these arguments we have concluded that the hydrogen bubbles were homogeneously nucleating at an atomically smooth electrode surface. The effect of the electric field on the surface tension within the double layer is suggested as the major reason for the observed discrepancy. A lowering in the surface tension would be consistent with our experimental results. Perhaps the effect of the electric field around motes in polar solvents accounts for the trouble with water in nucleation experiments.

## APPENDIX: NOMENCLATURE

$C_0$ equilibrium concentration of gas dissolved in the solvent (gmole/cm$^3$)

$\underline{C}_0$ equilibrium concentration of dissolved gas (gmole gas/gmoles solvent)

$C_s$ surface concentration of hydrogen at the center of the mercury pool (gmole/cm$^3$)

$C_{\infty 1}$ bulk concentration of hydrogen in aqueous phase (gmole/cm$^3$)

$C_{\infty 2}$ bulk concentration in mercury phase (gmole/cm$^3$)

$C'$ concentration of hydrogen in solution (gmole/cm$^3$)

$C'_{exp}$ experimentally determined concentration of hydrogen at the mercury pool surface (gmole/cm$^3$)

$C'_{th}$ predicted supersaturation concentration of hydrogen from classical nucleation theory (gmole/cm$^3$)

$D_{H_2}$ diffusion coefficient of hydrogen (cm$^2$/s)

$F$ Faraday's constant (coulombs/equivalent)

$g_l(r)$ equilibrium radial distribution function of the liquid phase

$i$ current density (A/cm$^2$)

$J$ frequency of formation of nuclei per unit volume of liquid phase (s$^{-1}$)

$k$ Boltzmann's constant (erg/K)

$k_i$ mass transfer coefficient of species $i$ (cm/s)

$m$ coefficient of linear axial velocity approximation (32) (s$^{-1}$)

$n$ equivalents per mole

$N_1$ mass transfer flux within aqueous phase (mole/s cm$^2$)

$N_2$ mass transfer flux within mercury phase (mole/s cm$^2$)

$P'$ pressure within the liquid phase (atm)

$P''$ pressure inside bubble nucleus (atm)

$P_\infty$ vapor pressure of pure solvent (atm)

$R_c$ critical radius of bubble nucleus (cm)

Sc Schmidt number

$T$ temperature

$V'(r)$ derivative of the potential of interaction (erg/cm)

$x_{ohp}$ position of outer Helmholtz plane (cm)

$Z$ frequency factor in the nucleation equation (s$^{-1}$)

$\lambda$ Debye length (cm)

$\mu$ viscosity (g/cm s)

$\nu_1$ activity coefficient of the solvent in the gas–vapor mixture

$\nu_2$ activity coefficient of the solute in the gas–vapor mixture

$\rho$ fluid density (g/cm$^3$)

$\sigma$ surface tension (dyn/cm)

$v'_1$ specific volume of pure solvent (cm$^3$/gmole)

$\phi$ potential within the diffuse double layer (V)

$\phi_{obp}$ potential at the outer Helmholtz plane (V)

ACKNOWLEDGMENT

This work was supported by the National Science Foundation.

REFERENCES

1. Volmer, M., and Weber, A., *Z. Phys. Chem.* **119,** 277 (1926).
2. Farkas, L., *Z. Phys. Chem.* **125,** 236 (1927).
3. Becker, R., and Doring, W., *Ann. Phys.* **24,** 719 (1935).
4. Doring, W., *Z. Phys. Chem.* **36,** 371 (1937).
5. Doring, W., *Z. Phys. Chem.* **38,** 292 (1938).
6. Zeldovich, Ya. B., *Acta Physicochim. URSS* **18,** 1 (1943).
7. Kagan, Yu., *Russ. J. Phys. Chem.* **34,** 42 (1960).
8. Frenkel, J., *Kinetic Theory of Liquids,* Dover, 1955.
9. Blander, M., and Katz, J. L., *AIChE J.* **21,** 833 (1975).
10. Ward, C. A., Balakrishnan, A., and Hooper, F. C., *Trans. ASME* **92,** 695 (1970).
11. Tucker, A. S., and Ward, C. A., *J. Appl. Phys.* **46,** 4801 (1975).
12. Apfel, R. E., *J. Chem. Phys.* **54,** 62 (1971).
13. Jarvis, T. J., Donahue, M. D., and Katz, J. L., *J. Colloid Interface Sci.* **50,** 359 (1975).
14. Mori, Y., Hijikata, K., and Nagatani, T., *Intl. J. Heat Mass Trans.* **19,** 1153 (1976).
15. Forest, T. W., and Ward, C. A., *J. Chem. Phys.* **66,** 2322 (1977).
16. Forest, T. W., and Ward, C. A., *J. Chem. Phys.* **69,** 2221 (1978).
17. Newman, J., "Electrochemical Systems," p. 146. Prentice-Hall, Englewood Cliffs, N. J., 1973.
18. Bowden, F. P., *Trans. Faraday Soc.* **23,** 571 (1927).
19. Bowden, F. P., and Rideal, E. K., *Proc. R. Soc. London Ser. A* **120,** 59 (1928).
20. Azzam, A. M., Bockris, J. O'M., Conway, B. E., and Rosenberg, H., *Trans. Faraday Soc.* **46,** 918 (1950).
21. Bockris, J. O'M., and Parsons, R., *Trans. Faraday Soc.* **44,** 860 (1948).
22. Frumkin, A., and Gorodetzkaja, A., *Acta Physicochim. URSS* **9,** 327 (1938).
23. Jofa, S., Kabanov, E., Kuchinski, E., and Chistyakov, F., *Acta Physicochim. URSS* **10,** 317 (1939).
24. Kabanov, B., and Ivanishenko, N., *Acta Physicochim. URSS* **6,** 701 (1937).
25. Post, B., and Hiskey, C. F., *J. Chem. Soc.* **72,** 4203 (1950).
26. Frumkin, A., *Acta Physicochim. URSS* **18,** 23 (1943).
27. Bowden, F. P., *Proc. R. Soc. London Ser. A* **126,** 107 (1929).
28. Knapp, R. T., *Trans. AMES* **80,** 1315 (1958).
29. Bockris, J. O'M., and Azzam, A. M., *Trans. Faraday Soc.* **48,** 145 (1952).
30. Wilkinson, M. C., *Chem. Rev.* **72,** 575 (1972).
31. Conway, B. E., Angerstein-Kozlowska, H., Sharp, W. B. A., and Criddle, E. E., *Anal. Chem.* **45,** 1331 (1973).
32. Dapkus, K. V., "Homogeneous Nucleation of Electrolytically Evolved Gases at an Ideal Electrode," Ph.D. dissertation. Carnegie-Mellon University, Pittsburgh, 1985.
33. Sides, P. J., *Intl. J. Multiphase Flow* **8,** 553 (1982).
34. Hirth, J. P., Pound, G. M., and Pierre, G., *Met. Trans.* **1,** 939 (1970).
35. Delahay, P., "Double Layer and Electrode Kinetics." Wiley, New York, 1965.
36. Grahame, D. C., *J. Chem. Phys.* **21,** 1054 (1953).
37. Kirkwood, J. G., and Buff, F. P., *J. Chem. Phys.* **17,** 338 (1949).
38. Schmid, G. M., and Snavely, Jr., E. S., *J. Electrochem. Soc.* **109,** 852 (1962).
39. Jalaluddin, A. K., and Sinha, D. B., *Del Nuovo Cimento Supp. X* **26,** 234 (1962).
40. Damm, E. P., *J. Electrochem. Soc.* **110,** 590 (1963).
41. Hayes, C. F., *J. Phys. Chem.* **79,** 1689 (1975).
42. Hurd, R. M., Schmid, G. M., and Snavely, Jr., E. S., *Science (Washington)* **135,** 791 (1962).
43. Rovin, Y. G., *Colloid J. USSR* **38,** 201 (1976).
44. Sacher, E., *J. Colloid Interface Sci.* **83,** 649 (1981).
45. Salt, R. W., *J. Inst. Physiol.* **2,** 178 (1958).
46. Salt, R. W., *Science (Washington)* **133,** 458 (1961).
47. Smolyak, B. M., and Brainin, M. I., *Colloid J. USSR* **42,** 224 (1980).
48. Rusanov, A. I., and Kuzmin, V. L., *Colloid J. USSR* **39,** 338 (1977).
49. Blander, M., Hengstenberg, D., and Katz, J. L., *J. Phys. Chem.* **75,** 3613 (1971).